Surprisingly Intense Neutron Emission from a Flare Behind the Limb of the Sun

R. J. Murphy and G. H. Share
E.O. Hulburt Center for Space Research, Code 7650, Naval Research Lab., Washington, DC 20375, U.S.A.

K. W. DelSignore
University of Michigan, U.S.A.

X.-M. Hua
GSFC, NASA/USRA, Greenbelt, MD 20771, U.S.A.

ABSTRACT

The Oriented Scintillation Spectrometer Experiment on board the *Compton Gamma Ray Observatory* observed a strong flux of neutrons from the behind-the-limb flare that occurred on 1991 June 1. This is surprising if the neutrons were produced by *thin target* interactions in the Sun's corona as suggested by γ-ray observations made by *Granat*/PHEBUS of this flare. We compare neutron and γ-ray observations of the June 1 flare with *thick target* emissions observed from a flare three days later where the interactions took place in the chromosphere and photosphere. A very hard spectrum for the accelerated particles is required to account for the number of neutrons observed on June 1 if they were produced by thin-target interactions in the corona.

Subject headings: Sun: flares — Sun: X-rays, gamma rays — Sun: abundances — acceleration of particles

1. INTRODUCTION

Most flares that emit detectable γ-ray and neutron emissions occur on the visible disk of the Sun. While it is generally believed that particle acceleration in flares takes place in the corona, interactions producing γ rays and neutrons are thought to occur predominantly in compact regions at the footpoints of magnetic loops. These *thick-target* interactions are believed to occur in the lower chromosphere or upper photosphere at densities $>10^{12}$ cm^{-3} (Chupp 1984). Because thick-target γ-ray line and neutron production is relatively

efficient, such emission from flares occurring on the solar disk is expected to overwhelm any *thin-target* emission from particles traversing the low-density coronal portions of magnetic loops. If the flare is located at or behind the limb, however, part or all of the thick-target emission could be occulted leading to a higher coronal contribution. Observations of γ-rays from over-the-limb flares are rare.

An example is the 1981 April 27 flare where Hα observations suggested that it occurred between 0 and 5° beyond the limb, corresponding to an occulting height of <3000 km above the photosphere (Takakura et al. 1983). In their X-ray–γ-ray timing analysis of this flare, Hulot et al. (1992) found that >30% of the strong γ-ray line flux observed with the Gamma Ray Spectrometer (GRS) aboard the *Solar Maximum Mission* (*SMM*) satellite could have been produced in the corona.

Another example of a behind-the-limb γ-ray producing flare was observed with *SMM*/GRS on 1989 September 29 (Vestrand and Forrest 1993). Vestrand and Forrest placed the location of the flare between 5 and 15° beyond the west limb of the Sun, corresponding to an occultation height between 3000 and 20,000 km. What was extraordinary for this flare was the detection of a strong 2.223 MeV neutron-capture line. This line is formed when flare-produced neutrons are captured on ambient H. Because the density must be high enough for the neutrons to slow down and be captured before decay, the line is only produced deep in the photosphere (Hua and Lingenfelter 1987a). For flares close to the limb of the Sun, the 2.223 MeV line is therefore strongly attenuated relative to the nuclear deexcitation lines produced at higher altitudes. This led Vestrand and Forrest to propose that energetic particles propagated from beyond the limb to impact over a spatially-extended area, including part of the visible disk, producing thick-target emission. The authors suggested that this might occur in the presence of a giant magnetic loop that reached around the limb to place a footpoint in the visible hemisphere. They also suggested this could result from a large, diffuse interaction region extending over the limb as might be produced by "back-diffusion" of particles accelerated over a large range of heliolongitudes by a coronal mass ejection. For this flare, then, the thick-target γ-ray line emitting region again dominated any coronal radiation from the loops of the flaring region behind the limb.

One of the most intense flares ever recorded emanated from Active Region 6659 on 1991 June 1 when it was located 6–9° beyond the east limb of the Sun (Barat et al. 1994) corresponding to an occultation height between 3000 and 7000 km above the photosphere. The flare was well-observed by the Solar X-ray/Cosmic Gamma-Ray Burst Experiment aboard the interplanetary spacecraft *Ulysses* (Kane et al. 1995), located 22° beyond the east limb of the Sun. Kane et al. (1995) estimated that the total energy released in the flare by >20 keV electrons was $\sim 10^{34}$ ergs with an energy release rate of ~2% of the total

solar luminosity. Thus, the June 1 flare was the largest flare of Cycle 22 and prompted Kane et al. to question whether the material and energy resources of the active region were adequate.

The June 1 flare was also observed (Barat et al. 1994) by the PHEBUS instrument on *Granat* in Earth orbit. In spite of the flare location, hard X rays and γ rays were observed through the peak of emission. The observed spectrum showed excesses above a bremsstrahlung power law in the 1.1–1.8 and the 4.1–7.6 MeV regions consistent with nuclear line emission. No significant 2.223 MeV neutron-capture line was detected.

The June 1 flare could have had a geometry similar to the 1989 September 29 flare discussed above in that a separate or extended region of thick-target emission on the visible disk produced the γ rays. The lack of a detectable 2.223 MeV line could be understood if the region were confined near the limb as in other γ ray-producing limb flares where the line is strongly attenuated such as the 1980 June 21 (Chupp et al. 198X) and 1981 April 27 (Murphy et al. 1990) flares observed with SMM. (The June 21 flare also produced neutrons similar to the June 1 flare.) If so, the June 1 γ-ray emission would be expected to have the spectral characteristics of thick target emission as observed in such limb flares. However, the June 1 γ-ray spectrum measured (Ramaty et al. 1997) by PHEBUS was very different in that the 1.1–1.8 MeV/ 4.1–7.6 MeV ratio was exceptionally high. This led Ramaty et al. (1997) to argue that such a high ratio is only possible from *thin-target* interactions occurring in the corona with accelerated particles having heavy-element ($>^{16}$O) abundance enhancements typical of energetic particles in impulsive events observed in interplanetary space. (This supported the conclusion of Barat et al. [1994] of a coronal source for the γ rays based on the lack of evidence of a large-scale magnetic loop system connecting the active region behind the limb to the visible disk.) Such thin-target interactions, however, are considerably less efficient in producing γ rays than are thick-target interactions. If the bulk of the emission from the June 1 flare was from the corona as suggested, the strong γ-ray signal detected apparently resulted from its phenomenal size.

An unexpected feature of this flare is that energetic neutrons were detected in low earth orbit by the Oriented Scintillation Spectrometer Experiment (OSSE) on board the *Compton Gamma Ray Observatory* (*CGRO*). Flare neutrons are produced by interactions of particles with energies typically greater than about 50 MeV nucleon^{-1}. Neutrons that are initially directed upward have a good chance of escaping from the solar atmosphere without scattering, and those that are initially directed downward lose most of their energy in the atmosphere with little chance of escape (Hua and Lingenfelter 1987b). Such downward-directed neutrons either decay at the Sun or are captured by nuclei at the Sun (see the 2.223 MeV line discussion above). The escaping neutron flux at Earth is extended

in time due to velocity dispersion and attenuated due to neutron decay. Because the probability of scattering in the corona is small and because any scattered neutrons would be of such low energy (Hua and Lingenfelter 1987b) that they would not survive the 1-AU distance, we do not expect the observed neutron flux to contain a significant contribution from neutrons produced by occulted thick-target interactions.

Detection of neutrons from flares is rare, even from thick-target disk flares, and thin-target interactions are even less efficient in producing neutrons than the thick-target interactions of disk flares. Thus the strong neutron flux observed from the June 1 flare, if also produced by the thin-target interactions believed responsible for the γ-ray emission, is surprising. In this paper we describe the OSSE detection of neutrons from this flare and determine whether thin-target interactions can account for the high flux. We do this by comparing the neutron counts and γ-ray fluence observed from the June 1 flare with the same quantities observed by OSSE from the thick-target disk flare that occurred three days later on June 4 while OSSE was pointed at the Sun. The June 4 flare was well observed by OSSE and both γ-rays over a broad spectral range (from 0.1 to $\sim$ 100 MeV) and neutrons were detected (Murphy et al. 1997; DelSignore 1995). The >15 MeV γ-ray emission observed from this flare was much more impulsive than the long-lasting 4–7 MeV nuclear emission, falling below detectability within 250 s after the γ-ray peak. The spectrum of the high-energy γ-ray emission showed no evidence for a pion-decay feature, implying that the emission was predominantly electron bremsstrahlung. A strong neutron signal was detected following the high-energy γ-ray emission and continued until the Sun was occulted by the Earth.

The June 1 and June 4 flare comparison will establish a *neutron-production efficiency* for June 1 relative to a known thick-target disk flare. This relative *efficiency* will then be compared with predicted thin-target *neutron efficiencies* calculated at a variety of accelerated-particle spectral indexes and the predicted thick-target *efficiency* calculated at the known spectral index determined (Murphy et al. 1997) for the June 4 flare. The comparison will show that thin-target interactions of accelerated particles are not adequate to account for the number of neutrons observed from the June 1 flare unless the spectrum is extremely hard (a power-law index <2). In §2, the OSSE response to neutrons is discussed. The flare observations are discussed in §3 and the results are given in §4. §5 provides a summary.

2. OSSE Response to Neutrons

The four 10 cm thick $\times$ 750 cm^2 NaI detectors provide OSSE with significant stopping power for high-energy neutrons. The effective area of each of these detectors is about 120 cm^2 (DelSignore 1995). Both high-energy γ-rays and neutrons can be detected and are distinguished by their different pulse shapes in NaI (Share et al. 1978); the rise-time to maximum amplitude for energy losses by the low energy protons, alpha-particles, etc. produced by neutron interactions is significantly shorter than that for energy losses by the electrons produced by γ-ray interactions. Pulse-shape discrimination is therefore used to distinguish neutron and γ-ray events and their energy-loss spectra are separately accumulated in 16 channels up to about 220 MeV for neutrons and about 150 MeV for γ rays (Johnson et al. 1993, DelSignore 1995). (We note that because the scintillation light output of a neutron interaction is less than that of a γ ray of the same energy, a given neutron spectral channel corresponds to a higher energy loss than that of the equivalent γ-ray channel.) The dotted histogram of Figure 1 shows the distribution of pulse durations for channel 3 of the 16-channel spectra obtained at the peak the 1991 June 4 flare when the emission is due to γ rays only. The solid histogram shows the distribution of durations for channel 3 obtained late in the flare after the high-energy γ-ray emission had dropped below detectability and only neutrons were present. (Channel 3 corresponds to 26–36 MeV energy losses for γ rays and 36–49 MeV energy losses for neutrons.) The dashed lines indicate the pulse-duration acceptance window for γ rays; all events with durations falling to the left of the window are categorized as neutrons. The ability to separate neutrons and γ rays is demonstrated although there is some overlap which increases with energy. Ground-based and in-orbit calibrations are used to correct for this overlap.

An instrument model for neutrons has been developed (DelSignore 1995), but for the purposes of this paper we require only information on the relative angular response of the OSSE detectors. A prototype OSSE detector was exposed to neutrons produced at the Indiana Cyclotron (Jenkins et al. 1991). The angle-dependent response of the detector at two relevant energies is plotted in Figure 2. We note for later use that the response at 100° is $\sim$70% of the on-axis response. We will confirm this measurement using data taken during the 1991 June 4 flare (§3).

3. OBSERVATIONS

An overview of the June 1 flare is shown in Figure 3. The top curve shows the GOES 1–8 Å soft X-ray emission which was saturated because of the intense flux. The bottom curve shows the count rate of hard X-rays (>27 keV) observed by *Ulysses* (Kane et al.

1995). The data points show the 1.1–1.8 and 4.1–7.6 MeV nuclear γ-ray fluxes (excess above a bremsstrahlung power-law continuum) observed by *Granat*/PHEBUS (Trottet et al. 1996). The γ-ray data are binned into 128-s intervals from 14:59:38 to 15:13:09 (53978 to 54789 s) UT. The line emission appears to peak during the third interval starting at 15:03:54 (54234 s) UT about 250 s before the peak of the hard X-rays observed by *Ulysses*. OSSE data are not available during this peak portion of the flare because *CGRO* was in the high radiation zone of the South Atlantic Anomaly (SAA) at that time. When observations resumed at $\sim$750 s after the peak of the γ-ray emission (55049 s UT), OSSE was pointed $\sim$100° away from the Sun observing the black hole candidate Cygnus X-1. Earth occultation of the Sun occurred about 260 s later (55312 s UT). The OSSE observation interval is indicated in the Figure by dotted lines.

OSSE has some response to γ-rays above 1 MeV even at this large offset angle ($\sim$20% of the on-axis response). Because of SAA contamination, however, a reliable background-subtracted spectrum could not be obtained so a 4–7 MeV nuclear line flux could not be directly derived. The 4–7 MeV count rate did show a sudden decrease at the time of satellite night suggesting that γ-ray emission from the Sun was detected. The magnitude of the change in this count rate was converted to a photon flux using an estimate for the 100° off-pointed effective area at 4–7 MeV. The resulting flux is plotted in Figure 3. It is shown as an upper limit to the 4–7 MeV nuclear γ-ray flux because (1) it includes an unknown contribution from electron bremsstrahlung and (2) there may be some contamination of the count rate at these energies due to energy losses of higher-energy solar neutrons. A fit to the OSSE data at this time for the narrow 2.223 MeV neutron-capture line indicated no significant flux, with a 2-σ upper limit of 1×10^{-2} photons cm^{-2} s^{-1}.

Surprisingly, a decrease at satellite night in the rate of >15 MeV events attributed to neutrons was also observed. Plotted in Figure 4 are the background-subtracted rates in the neutron channel. Background was obtained from observations approximately 15 orbits after the flare observation when orbital conditions (location and aspect to the Earth) were similar. We were not able to use the average of rates 15 orbits both before and after the flare as is usual because parameters affecting the neutron-γ-ray separation were set differently on the previous day. This one-sided background prediction was tested during flare quiet times and successfully produced null difference spectra. The uncertainties shown in Figure 4 are statistical. After satellite night, the background-subtracted rate fell to zero as expected for a solar source.

A key question is whether this high-energy emission is indeed due to neutrons. Because the OSSE neutron-γ-ray distinction via pulse-shape discrimination is not perfect (see §2), a fraction of neutron events are counted as neutrons and the complement as γ rays. The

analogous situation holds true for γ-ray events. The true neutron and γ-ray energy-loss spectra in channels 3 through 7 (36–100 MeV neutron and 15–65 MeV γ-ray energy losses) can be recovered by using the separation constants developed by DelSignore (1995). (Above channel 7, the neutron-γ-ray distinction is too poor to allow reliable separation.) The separated channels 3–7 neutron and γ-ray energy-loss spectra for Detector 1 are shown in Figure 5 and clearly show that the high-energy emission detected by OSSE from the June 1 flare is indeed due predominantly to neutrons. No high-energy γ-ray data are available during the peak of emission, but the OSSE data indicate that any >15 MeV γ-ray emission late in the June 1 flare was below detectability by the OSSE detectors.

Time profiles of nuclear γ-rays and count rates attributed to neutrons from both the 1991 June 1 and the 1991 June 4 flares are shown in Figure 6. In this plot, the bottom time axis is for the June 1 flare and the top time axis is for the June 4 flare. The 4.1–7.6 MeV nuclear γ-ray fluences observed by *Granat*/PHEBUS (Trottet et al. 1996) for the June 1 flare and by OSSE for the June 4 flare are binned into 128- and ∼131-s intervals, respectively. The background-subtracted neutron count rates observed by OSSE for the June 1 flare are binned into ∼16-s intervals and for the June 4 flare are binned into ∼8-s intervals when pointed at the Sun and ∼16-s intervals after OSSE rotated away from the Sun and pointed at Cygnus X-1. Earth occultation of the Sun on June 4 occurred ∼230 s after repointing. Background estimation for the June 4 neutron data was derived using data obtained 15 orbits before and 15 orbits after the observation. The June 4 neutron count rate fell to zero at satellite night as expected for a solar source. The time axis for the June 4 flare data has been shifted so that the peak of the June 4 γ-ray emission (dotted line at ∼13270 s UT on June 4) coincides with the mid-point of the time bin containing the peak of the June 1 γ-ray emission.

Because the OSSE detectors were pointed 100° away from the Sun during the June 1 observation but were pointed at the Sun during the June 4 observation, the June 1 neutron count rates must be corrected relative to those of June 4 to account for the reduced detector efficiency. As mentioned in §2, the laboratory calibration of Jenkins et al. (1991) indicated that the response at 100° is ∼70% of the on-axis response. We confirm this using the June 4 neutron data. The dotted line in Figure 6 associated with the June 4 neutron data indicates the end of solar-pointing and the onset of motion as the OSSE detectors rotated ∼100° away from the Sun to acquire Cygnus X-1. Rotation was complete in about 50 s. Linear fits to the data obtained both before and after detector movement were performed. Extrapolations of these fits to the midpoint of detector motion imply that the off-pointed effective area is $(70 \pm 13)\%$ of the on-pointed area, confirming the calibration. The June 1 neutron count rates shown in Figure 6 have been corrected for this reduced OSSE off-axis response. The uncertainties plotted are statistical; the systematic uncertainty due to

this off-axis correction will be added in quadrature with the statistical uncertainty in the analysis that follows.

Since we are comparing neutron count rates with 4–7 MeV fluences that have been obtained with different instruments, the relative γ-ray calibration of the two detectors must also be considered. Coincident data are available for the 1991 June 11 flare (Barat and Trottet, private communication) when both instruments observed the peak of emission and OSSE was in the same observing configuration as for the June 4 flare. The mean 4–7 MeV nuclear γ-ray fluences derived with the two instruments were consistent to within 12% ($<$1.3 σ difference). We will also include this additional uncertainty in the analysis that follows.

4. RESULTS

We compare the high-energy neutron count rates and the 4–7 MeV nuclear γ-ray fluences for the two flares. For the neutrons, we integrated the June 4 rates over a 280-s interval at approximately the same time following the June 4 γ-ray peak as was available for the June 1 flare (see Figure 6). Because the neutron flux is changing slowly at the time of interest, a small shift in this accumulation interval will not significantly affect the results. The total integrated neutron counts are 1430 $\pm$ 270 for the June 1 flare (corrected for off-axis angular response) and 4720 $\pm$ 45 neutrons for the June 4 flare.

The 4–7 MeV γ-ray time profiles of the two flares are similar (see Figure 6), although the fluxes are significantly different. During the $\sim$800 s interval defined by the dashed-dotted lines in Figure 6, the measured 4.1–7.6 MeV nuclear fluences are 89 $\pm$ 7 photons cm^{-2} for the June 1 flare (Trottet et al. 1996) and 649 $\pm$ 4 photons cm^{-2} for the June 4 flare. The uncertainties are statistical.

We define a *neutron efficiency*, η, as the ratio of observed neutron counts to observed 4.1–7.6 MeV nuclear γ-ray fluence. For the June 1 flare, $\eta_{\rm June\ 1} = 16.2 \pm 5.1$ and, for the June 4 flare, $\eta_{\rm June\ 4} = 7.3 \pm 0.1$. In estimating the June 1 efficiency, we have included the systematic uncertainty associated with the 4–7 MeV intercalibration of the OSSE and *Granat*/PHEBUS detectors and the off-axis neutron response correction as discussed above. The ratio of these two efficiencies, $\eta_{\rm June\ 1}/\eta_{\rm June\ 4}$, shows that the June 1 *thin-target* flare was more efficient in producing neutrons than the June 4 *thick-target* flare by a factor of 2.2 $\pm$ 0.5. We note that if the June 1 OSSE neutron observation did not occur near the peak of the neutron count rate as did the corresponding June 4 neutron observation (see Figure 6), this factor would be higher, implying that the value of 2.2 is actually a *lower* limit.

We wish to compare this *neutron efficiency* ratio of the two flares,

$\eta_{\rm June\ 1}/\eta_{\rm June\ 4} = 2.2 \pm 0.5$, with predicted ratios of thin- and thick-target *neutron efficiencies*, $\eta_{\rm thin}/\eta_{\rm thick}$, for power-law accelerated-particle spectra. For the ambient material, we assume a coronal composition (Reames 1995). Gamma-ray measurements of other flares (Murphy et al. 1991; Ramaty et al. 1995; Ramaty et al. 1996; Murphy et al. 1997) have shown that the ambient flare material typically has the low First Ionization Potential elemental abundance enhancements found in the corona and solar wind. For the accelerated particles, we assume the mean composition (Ramaty et al. 1996) of impulsive flares observed in interplanetary space (with accelerated α/proton ratios of either 0.1 or 0.5). This impulsive-flare composition is considerably different from photospheric or coronal abundances, having significant enhancements of Ne, Mg, Si and Fe in addition to ^{3}He/α = 1. In our analysis of the June 4 flare (Murphy et al. 1997), we found such an enhanced high-Z accelerated-particle composition was necessary to achieve agreement between the two techniques of determining accelerated-particle spectral indexes: the neutron-capture-^{12}C 4.44 MeV line fluence ratio and the ^{16}O 6.13 MeV-^{20}Ne 1.63 MeV line fluence ratio. This was consistent with the 1981 April 27 flare analysis of Murphy et al. (1991) and the 19 *SMM*/GRS flare analysis of Ramaty et al. (1996). In their analysis of the *Granat*/PHEBUS γ-ray data from the June 1 flare, Ramaty et al. (1997) also found that the accelerated particles showed heavy-element enhancements. We use the calculations of Ramaty et al. (1996) for the thick-target neutron yield. For the thin-target neutron yields and the thin- and thick-target 4–7 MeV nuclear γ-ray yields, we use results of new calculations which will be published elsewhere.

Shown in Figure 7 is the predicted ratio $\eta_{\rm thin}(s_{\rm thin})/\eta_{\rm thick}(s)$ where $\eta_{\rm thin}(s_{\rm thin})$ is the thin-target *neutron efficiency* calculated as a function of accelerated-particle spectral index $s_{\rm thin}$ and $\eta_{\rm thick}(s)$ is the thick-target *neutron efficiency* calculated at either of two spectral indexes derived (Murphy et al. 1997) for the June 4 flare: $s = 3.7 \pm 0.1$ and $s = 4.2 \pm 0.1$. These June 4 indexes were derived using the measured fluence ratio of the 2.223 MeV neutron-capture and 4.44 MeV ^{12}C lines and the thick-target calculations of Ramaty et al. (1996). The harder index (3.7) was derived assuming $\alpha/p = 0.1$ and the softer index (4.2) was derived assuming $\alpha/p = 0.5$. The lower value of α/p results in a lower *neutron efficiency* which must be balanced by a harder energetic-particle spectrum.

The observed June 1-to-June 4 *neutron efficiency* ratio, $\eta_{\rm June\ 1}/\eta_{\rm June\ 4}$, is compared with the predicted *efficiency* ratios in Figure 7. This comparison shows that thin-target interactions of particles can produce sufficient neutrons only if the accelerated-particle spectrum is extremely hard, with an index <1.8 (for $\alpha/p = 0.1$, $s = 3.7$) and <2.0 (for $\alpha/p = 0.5$, $s = 4.2$).

5. SUMMARY

Because the magnetic loop footpoints associated with the 1991 June 1 behind-the-limb flare were hidden from view, the nuclear γ-ray emission observed (Barat et al. 1994) with *Granat*/PHEBUS has been interpreted as originating from the corona over the active region. Furthermore, because of the exceptionally high ratio of the 1.1–1.8 MeV to 4.1–7.6 MeV excesses observed from this flare, the emission is thought (Ramaty et al. 1997) to have resulted from *thin-target* interactions of accelerated particles with impulsive-flare abundances, lending support to the coronal hypothesis. *CGRO*/OSSE also observed neutrons from this flare. Neutron production in flares is rare, even from the thick-target interactions of disk flares. Since thin-target interactions are even less efficient in producing neutrons than thick-target interactions, the strong neutron signal observed from this flare is surprising.

In this paper, we compared the neutron counts observed by OSSE and the nuclear γ-ray fluence observed by *Granat*/PHEBUS from the 1991 June 1 flare with the same quantities observed with OSSE alone from the 1991 June 4 flare that occurred on the disk. The comparison establishes a *neutron-production efficiency* for the June 1 thin-target flare relative to a known thick-target disk flare. This relative *efficiency* was compared with predicted ratios of thin-target *neutron efficiencies* (calculated at a variety of spectral indexes) to thick-target *efficiencies* (calculated at the spectral indexes determined previously [Murphy et al. 1997] for the June 4 flare). The calculations were performed assuming average impulsive-flare abundances (Ramaty et al. 1996) for the accelerated particles and coronal abundances (Reames 1995) for the ambient medium.

The comparison in Figure 7 shows that thin-target interactions of accelerated particles are not adequate to account for the number of neutrons observed from the June 1 flare unless the accelerated-particle spectrum is extremely hard, with a power-law index s_{thin} <2.0. In their thin-target analysis of the *Granat*/PHEBUS 1.1–1.8 and 4.1–7.6 MeV γ-ray observations of the June 1 flare, Ramaty et al. (1997) obtained a spectral index as hard as $s_{thin} \simeq 2.5$ for the 10–30 MeV accelerated particles (assuming average impulsive-flare abundances) and possibly harder than 2 (assuming the highest observed heavy-element enhancements). Our analysis of the OSSE neutron data has shown that such a hard spectrum continues to energies >50 MeV.

For the first three of the intense flares of June 1991 (June 1, 4, and 6), the Sun was outside the field of view of the EGRET spark chamber. After the target of opportunity was declared, *CGRO* was reoriented, allowing the spark chamber to observe the June 9 and 11 flares. The June 11 flare in particular was remarkable in that the high-energy γ-ray emission continued for 8 hours (Kanbach et al. 1993). For both the June 1 and June

4 flares, the OSSE >15 MeV data indicate that by 750 s after the peak of the nuclear γ-ray emission, the high-energy γ-ray emission had fallen to below detectability. If these flares had produced high-energy γ-ray emission as intense and temporally extended as that observed by EGRET from the June 11 flare, OSSE would have detected it at a significance of $\sim 8\ \sigma$ from the June 4 flare and $<2\ \sigma$ from the June 1 flare (due to the reduced $\sim 100^\circ$ off-pointed sensitivity). Also, the spectrum of the June 4 emission at the peak of the flare was dominated by electron bremsstrahlung (DelSignore 1995, Murphy et al. 1997) rather than pion-decay radiation as in the June 11 flare. Thus the high-energy emission of at least the June 4 flare does not appear to be similar to that of the June 11 flare. Because no high-energy γ-ray data are available during the peak of the June 1 flare, it is not known whether such emission, if present, was due to electron bremsstrahlung or pion-decay. The very hard accelerated-particle spectrum derived for this flare, however, would suggest a strong pion-decay component.

We wish to acknowledge J. E. Grove, W. N Johnson, J. D. Kurfess, M. S. Strickman, G. V. Jung and D. Messina for their help in analyzing the OSSE data. XMH wishes to thank R. Ramaty for support of his work. Support for this work was provided by NASA DPR S-10987-C, NASA DPR S-92556-F and the Office of Naval Research.

REFERENCES

Barat, C., Trottet, G., Vilmer, N., Dezalay, J.-P., Talon, R., Sunyaev, R., Terekhov, O., and Kuznetsov, A. 1994, ApJ, 425, L109

Chupp, E. L., Forrest, D. J., Ryan, J. M., Heslin, J., Reppin, C., Pinkau, K., Kanbach, G., Rieger, E., and Share, G. H. 1982, ApJ, 263, L95

Chupp, E. L. 1984, ARA&A, 22, 359

DelSignore, K. W. 1995, Ph.D. thesis, Case Western Reserve University

Hua, X.-M., and Lingenfelter, R. E. 1987a, Sol. Phys., 107, 351

Hua, X.-M., and Lingenfelter, R. E. 1987b, ApJ, 323, 779

Hulot, E., Vilmer, N., Chupp, E. L., Dennis, B. R., and Kane, S. R. 1992, A&A, 256, 273

Jenkins, T. L., Frye, G. M., Stansfield, S., Kinzer, R. L., Jensen, C., Kurfess, J. D., Johnson, W. N., Strickman, M. S., Byrd, R., and Foster, C. 1991, 22nd Int. Cosmic Ray Conf. (Dublin), 3, 760

Johnson, W. N., Kinzer, R. L., Kurfess, J. D., Strickman, M. S., Purcell, W. R., Grabelsky, D. A., Ulmer, M. P., Hillas, D. A., Jung, G. V., and Cameron, R. A. 1993, ApJS, 86, 693

Kanbach, G., Bertsch, Fichtel, C. E., Hartman, R. C., Hunter, S. D., Kniffen, D. A., Kwok, P. W., Lin, Y. C., Mattox, J. R., Mayer-Hasselwander, H. A., Michelson, P. F., von Montigny, C., Nolan, P. L., Pinkau, K., Rothermel, H., Schneid, E., Sommer, M., Sreekumar, P., & Thompson, D. J. 1993, A&AS, 97, 349

Kane, S. R., Hurley, K., McTiernan, J. M., Sommer, M., Boer, M., and Niel, M. 1995, ApJ, 446, L47

Murphy, R. J., Share, G. H, Letaw, J. R., & Forrest, D. J 1990, ApJ, 358, 298

Murphy, R. J., Ramaty, R., Kozlovsky, B., and Reames, D. V 1991, ApJ, 371, 793

Murphy, R. J., Share, G. H., Grove, G. E., Johnson, W. N., Kinzer, R. L., Kurfess, J. D., Strickman, M. S., and Jung, G. V. 1997, ApJ, 490, 883

Ramaty, R., Mandzhavidze, N., Kozlovsky, B., and Murphy, R. J. 1995, ApJ, 455, L193

Ramaty, R., Mandzhavidze, N., and Kozlovsky, B. 1996, in AIP Conf. Proc. 374, High Energy Solar Physics, ed. R. Ramaty, N. Mandzhavidze, & X.-M. Hua (New York:AIP), 172

Ramaty, R., Mandzhavidze, N., Barat, C., and Trottet, G. 1997, ApJ, 479, 458

Reames, D. V. 1995, Adv. Sp. Res., 15, No. 7, 41

Share, G. H., Kurfess, J. D., and Theus, R. B. 1978, Nucl. Instr. Meth., 148, 531

Takakura, T., Tsuneta, S., Ohkhi, K., Nitta, N., Makishima, K., Murakami, T., Ogawara, Y., Oda, M., and Miyamoto, S. 1983, ApJ, 270, L83

Trottet, G., Barat, C., Ramaty, R., Vilmer, N., Dezalay, J.-P., Kuznetsov, A., Mandzhavidze, N., Sunyaev, R., Talon, R., and Terekhov, O. 1996, in AIP Conf. Proc. 374, High Energy Solar Physics, ed. R. Ramaty, N. Mandzhavidze, & X.-M. Hua (New York:AIP), 153

Vestrand, W. T., and Forrest, D. J. 1993, ApJ, 409, L69

This preprint was prepared with the AAS LaTeX macros v4.0.

Fig. 1.— Pulse duration distributions of neutron (solid) and γ-ray (dotted) events for channel 3 of the 16-channel energy-loss spectra. Channel 3 corresponds to energy losses of 36–49 MeV for neutrons and 26–36 MeV for γ rays. The dashed lines indicate the duration acceptance window for γ rays; all events with duration times falling to the left of the window are categorized as neutrons.

Fig. 2.— Relative neutron response as a function of incident angle for 32 and 83 MeV neutrons obtained from laboratory measurements performed with the OSSE instrument (Jenkins et al. 1991).

Fig. 3.— Overview of the 1991 June 1 solar flare. The upper curve is the GOES 1–8 Å soft X-ray emission, the bottom curve is the *Ulysses* >27 keV hard X-ray emission and the data points are the *Granat*/PHEBUS 1.1–1.8 and 4.1–7.6 MeV nuclear γ-ray excesses. The open diamond is the upper limit of the 4.1–7.6 MeV nuclear excess observed by OSSE. Also shown are the start time of the *CGRO*/OSSE observation and the onset of *CGRO* night.

Fig. 4.— The OSSE 1991 June 1 background-subtracted mean count rate per detector for events attributed to neutrons. The dotted line indicates when OSSE resumed observations of Cygnus X-1 after SAA exit and the dashed line shows the onset of *CGRO* night.

Fig. 5.— Separated channels 3–7 neutron and γ-ray energy-loss spectra derived from the OSSE June 1 high-energy data. Channels 3–7 correspond to 36–100 MeV neutron and 15–65 MeV γ-ray energy losses.

Fig. 6.— Nuclear γ-ray and neutron observations of the 1991 June 1 and 1991 June 4 flares. The bottom time axis is for the June 1 flare and the top time axis is for the June 4 flare. The June 1 neutron data have been corrected for the OSSE off-axis response. The peak of the June 4 γ-ray emission is shown by the dotted line and the June 4 time axis has been shifted so that this emission peak coincides with the mid-point of the time bin containing the peak of the June 1 γ-ray emission. Also shown are the accumulation intervals of the June 4 OSSE γ-ray and neutron data used in the analysis and the start time of detector motion away from the Sun during the June 4 flare.

Fig. 7.— Calculated ratios of thin- to thick-target *neutron efficiencies* as a function of accelerated-particle spectral index s_{thin} calculated at either of two thick-target spectral indexes (s) derived (Murphy et al. 1997) for the June 4 flare: $s = 4.2 \pm 0.1$ (assuming $\alpha/p = 0.5$; solid curves) and $s = 3.7 \pm 0.1$ (assuming $\alpha/p = 0.1$; dotted curves). Also shown is the observed June 1-to-June 4 *efficiency* ratio, $\eta_{\rm June\ 1}/\eta_{\rm June\ 4}$.

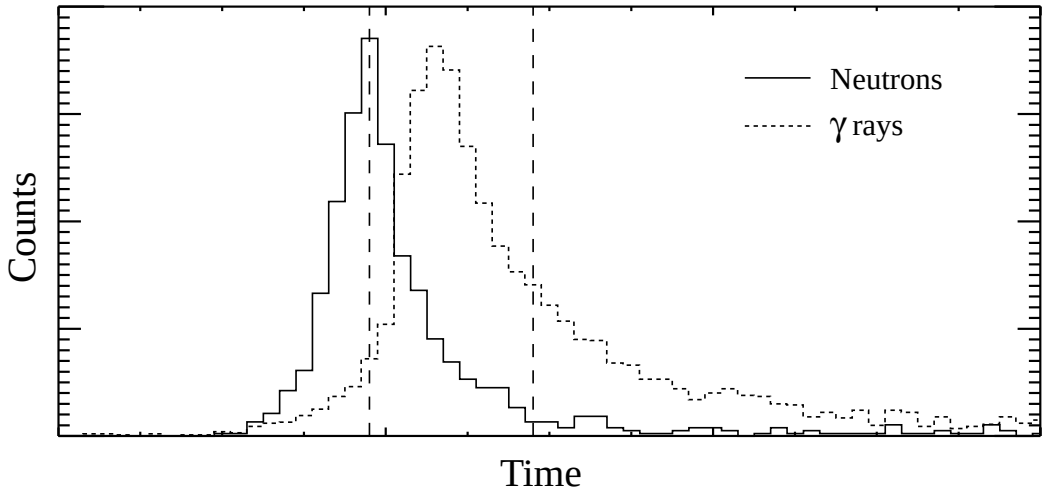

Figure 1

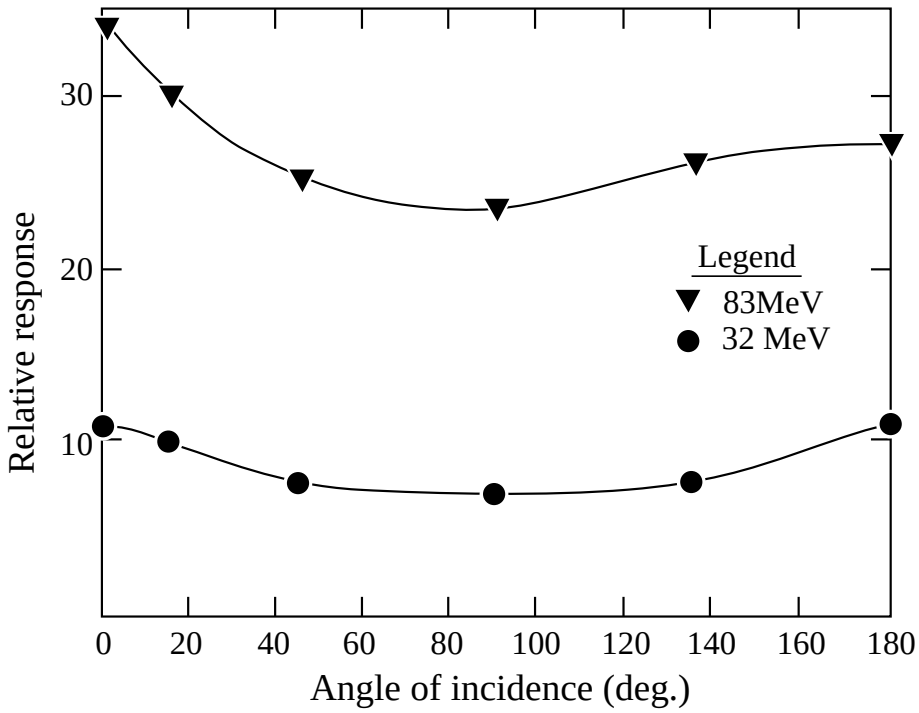
Relative response
30
20
10
0
20
40
60
80
100
120
140
160
180
Angle of incidence (deg.)
Legend
83MeV
32 MeV

Figure 2

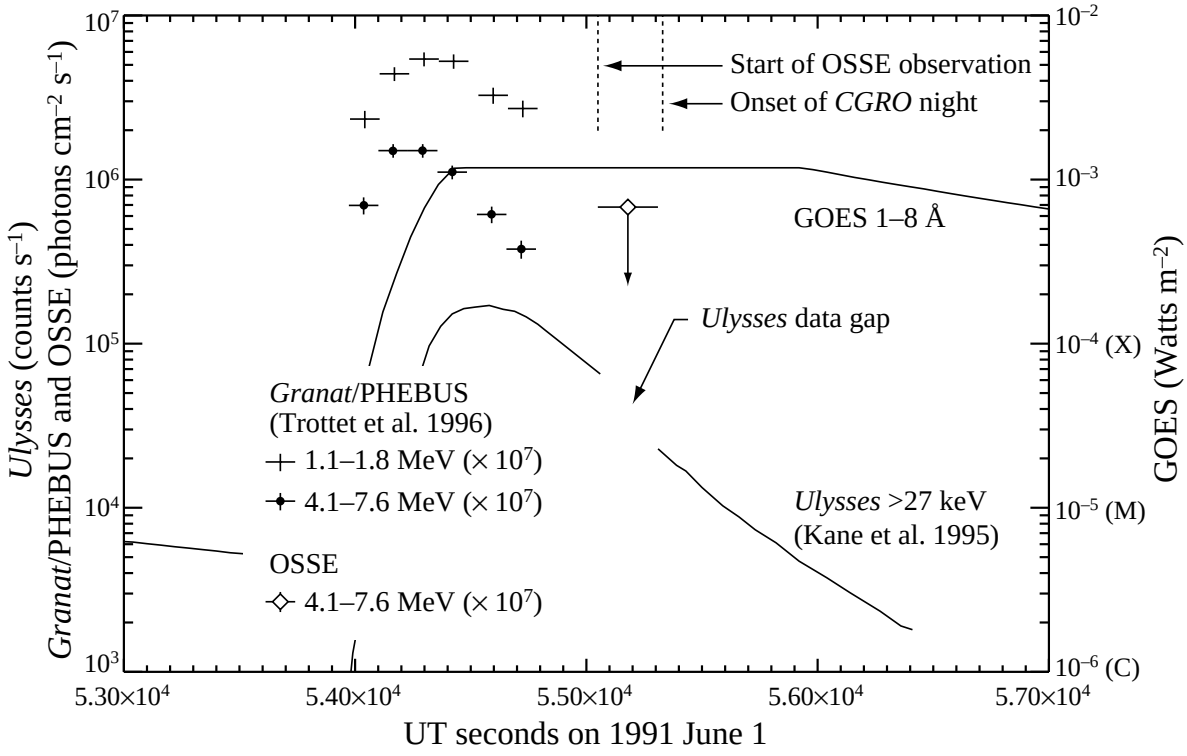
Start of OSSE observation
Onset of CGRO night
GOES 1–8 Å
Ulysses data gap
Granat/PHEBUS
(Trottet et al. 1996)
1.1–1.8 MeV (× 10^7)
4.1–7.6 MeV (× 10^7)
OSSE
4.1–7.6 MeV (× 10^7)
Ulysses >27 keV
(Kane et al. 1995)
Ulysses (counts s^−1)
Granat/PHEBUS and OSSE (photons cm^−2 s^−1)
GOES (Watts m^−2)
10^7
10^6
10^5
10^4
10^3
10^−2
10^−3
10^−4 (X)
10^−5 (M)
10^−6 (C)
5.30×10^4
5.40×10^4
5.50×10^4
5.60×10^4
5.70×10^4
UT seconds on 1991 June 1

Figure 3

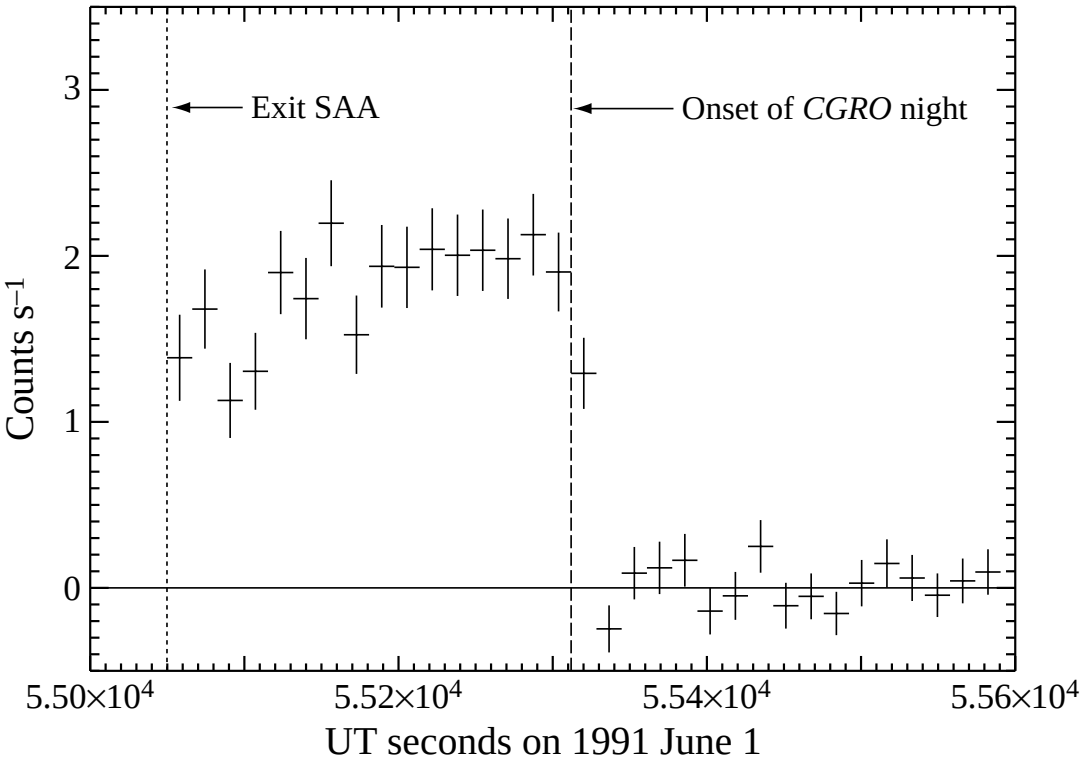
Exit SAA
Onset of *CGRO* night
Counts s^{-1}
3
2
1
0
5.50×10^4
5.52×10^4
5.54×10^4
5.56×10^4
UT seconds on 1991 June 1

Figure 4

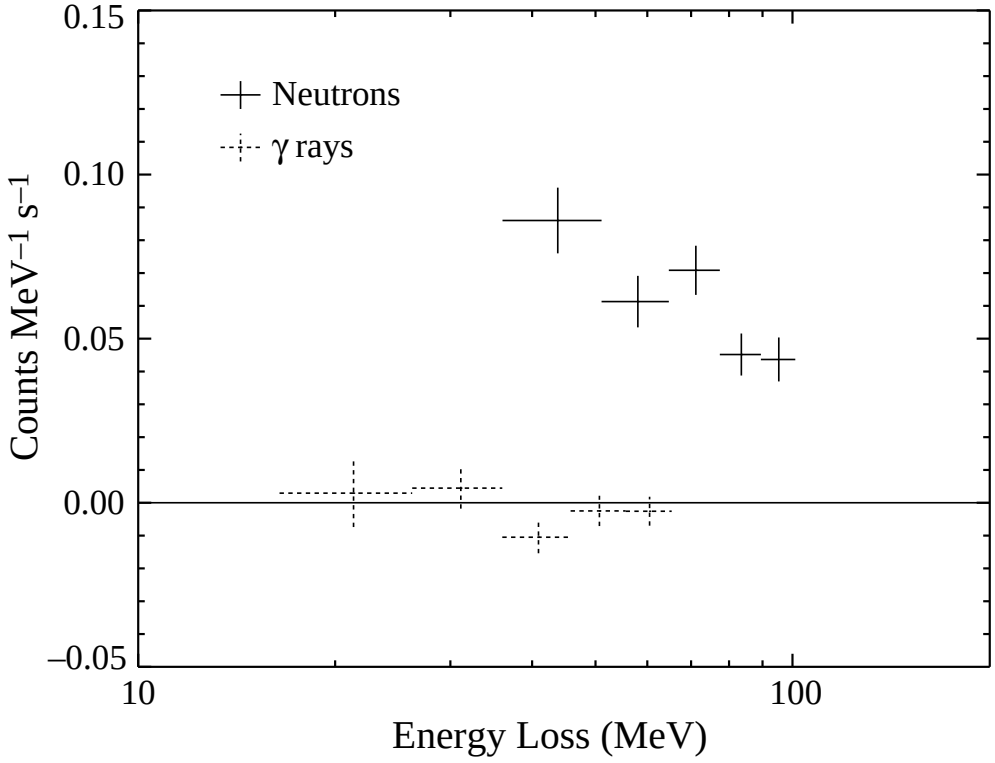
0.15
0.10
0.05
0.00
–0.05
Counts MeV⁻¹ s⁻¹
Neutrons
γ rays
10
100
Energy Loss (MeV)

Figure 5

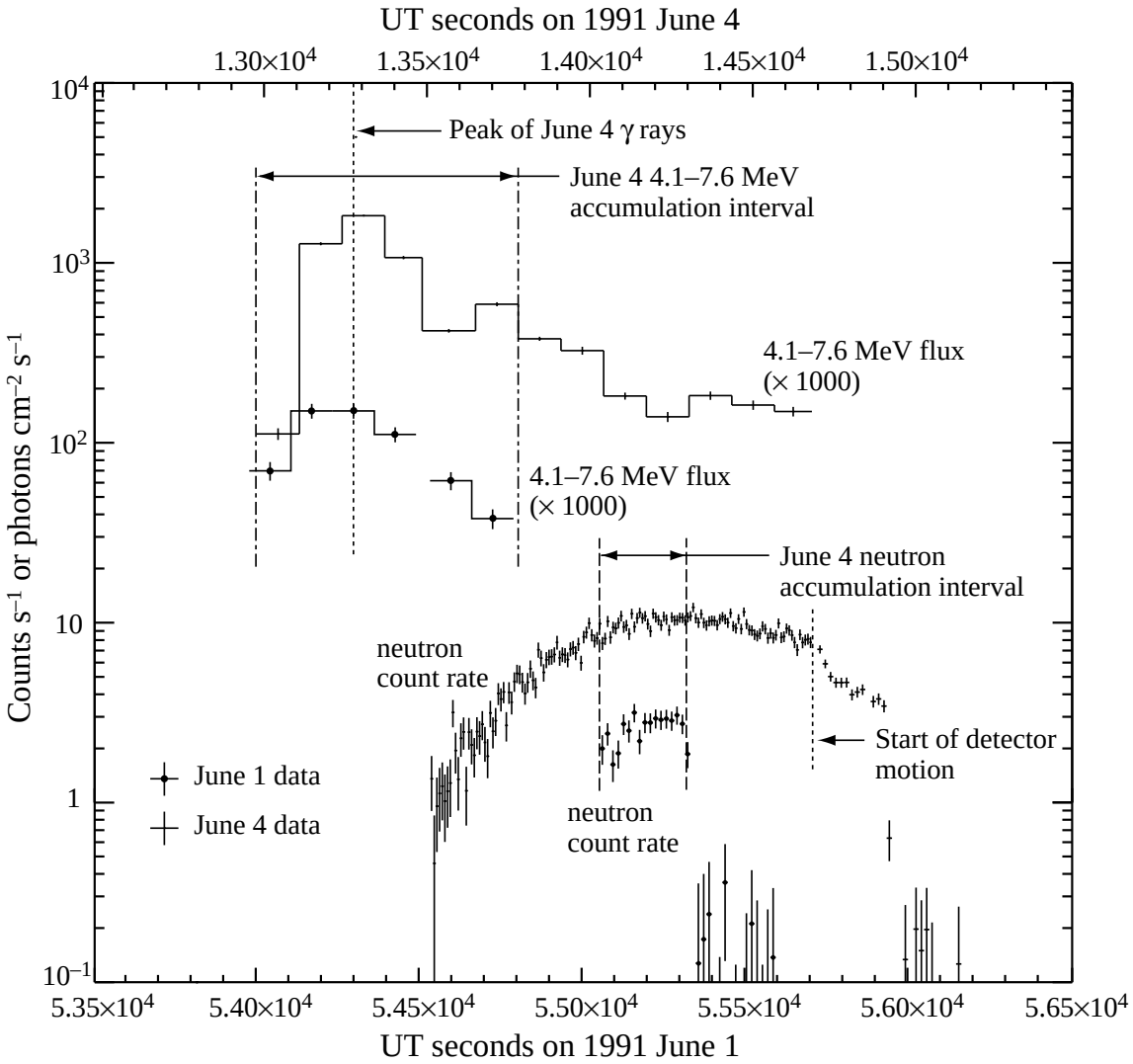
UT seconds on 1991 June 4
1.30×10^4
1.35×10^4
1.40×10^4
1.45×10^4
1.50×10^4
Peak of June 4 γ rays
June 4 4.1–7.6 MeV
accumulation interval
4.1–7.6 MeV flux
(× 1000)
4.1–7.6 MeV flux
(× 1000)
June 4 neutron
accumulation interval
neutron
count rate
neutron
count rate
Start of detector
motion
June 1 data
June 4 data
Counts s^−1 or photons cm^−2 s^−1
10^4
10^3
10^2
10
1
10^−1
5.35×10^4
5.40×10^4
5.45×10^4
5.50×10^4
5.55×10^4
5.60×10^4
5.65×10^4
UT seconds on 1991 June 1

Figure 6

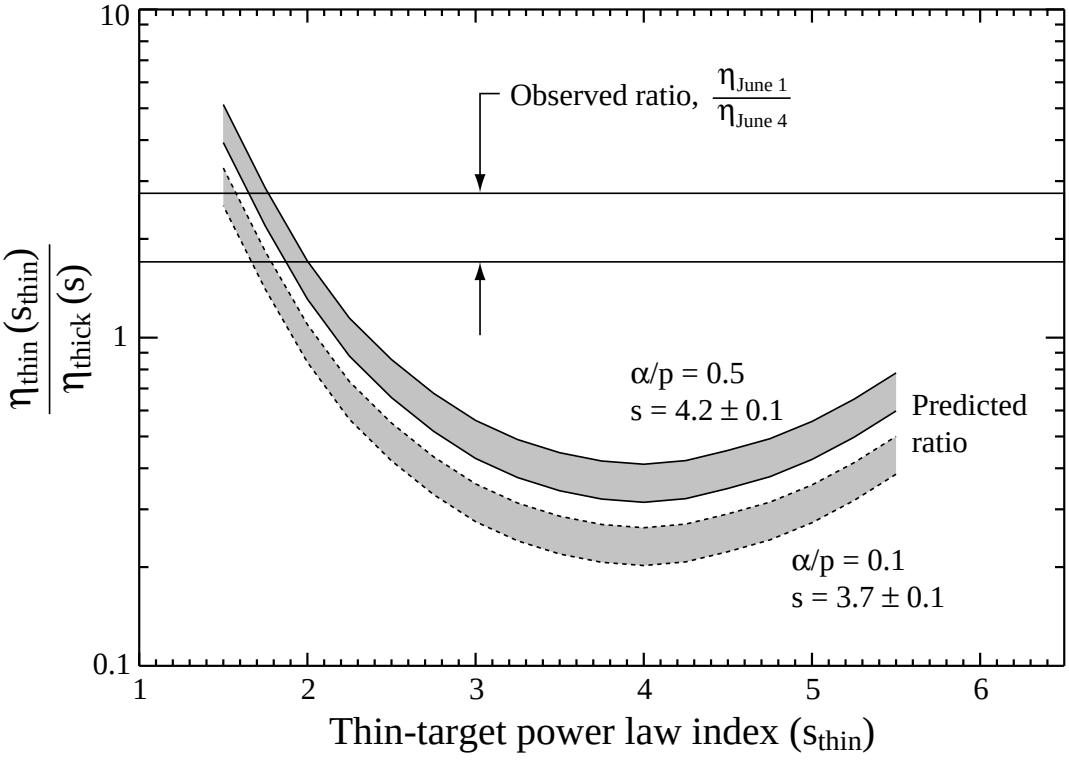
10
1
0.1
1
2
3
4
5
6
Observed ratio, $\frac{\eta_{\text{June 1}}}{\eta_{\text{June 4}}}$
$\alpha/p = 0.5$
$s = 4.2 \pm 0.1$
Predicted ratio
$\alpha/p = 0.1$
$s = 3.7 \pm 0.1$
$\frac{\eta_{\text{thin}}(s_{\text{thin}})}{\eta_{\text{thick}}(s)}$
Thin-target power law index (s_{thin})

Figure 7